

Rigorous Characterization of MMI-based Photonic Devices

M. Rarajan, B.M.A. Rahman, T. Wongcharoen, and K.T.V. Grattan
Department of Electrical Electronic and Information Engineering
City University
Northampton Square, London. UK. EC1V 0HB.
Tel: +44-171-477-8123 Fax : +44-171 477 8568
Email : B.M.A. Rahman@city.ac.uk

Abstract : In this paper multimode interference based devices such as 3dB couplers and duplexers are characterized and their performance characteristics in areas such as power coupling efficiency, excess loss and imbalance are discussed. It is also shown that the MMI-based device shows a better cross-talk performance and insensitivity to polarization when compared to a directional coupler-based device. Their modal propagation constants and the modal field profiles are obtained by employing the Finite Element (FE) method and the excited modal coefficients at the discontinuity interfaces are obtained by using the Least Squares Boundary Residual (LSBR) method.

1 Introduction

Today's evolving telecommunication systems demand a steadily increasing share of access networks. These networks are particularly demanding on high flexibility and reconfigurability, which requires enhanced functionality of photonic integrated circuits (PICs) for optical communications. In these optical systems, the key issue is the development of highly economic but reliable optoelectronic transceivers. In order to set up a bidirectional link on a single fiber transmission line, a passive duplexer is required at the transceiver modules for wavelength routing. On the other hand, 3dB optical power splitters are key components in many photonic integrated circuits, such as preamplified lightwave receivers using a Bragg reflection grating-folded noise filter, balanced coherent lightwave receivers, and optical switches. Due to the high power levels of the incoming and the outgoing signals, a significant level of isolation is required at the routing ports. This can be achieved by using a directional coupler section [1]. However, the device length increases as the separation between the two coupled wave guides increases. Duplexing can also be achieved by using a compact multimode interference (MMI) - based device [2], the basic function of which is to split and/or re-route the incoming light. Recently MMI-based devices have been gaining importance as they are more compact, less polarization-dependent, and less sensitive to fabrication tolerances as compared to directional coupler-based systems. In this paper, an accurate and numerically efficient approach is presented for the characterization of such MMI-based devices.

The vector finite element method (VFEM) is used to find the accurate modal solutions, the propagation constants and the vector field profiles of all the modes present in the input/output waveguide sections and also in the MMI-section. To find the transmission

and reflection coefficients, the least squares boundary residual (LSBR) method, which is also a rigorous vectorial approach, is applied. The combination of the VFEM and the LSBR is an accurate more efficient than the simpler mode-matching technique and also more efficient than the computer-intensive beam propagation method.

In this paper results are shown for the calculation of the power transfer efficiency and the fabrication tolerances for a 3-dB coupler. Data are also presented on *bar* and *cross-state* power transfer efficiency, for a compact optical duplexer using the *sol-gel* technique incorporating a MMI waveguide section. Finally, some key properties of MMI such as cross-talk and insensitivity to polarization are compared with those of the directional coupler.

2. Theory of the 3 dB coupler

Due to the multimode nature of the device, there is a large number of modes present in a typical MMI section. These modes will be excited by the incident fundamental mode entering through the access waveguide. Since the excited modes in the MMI section propagate with different phase velocities, they interfere with each other to form one or more interference patterns, the so-called '*self-images*' or '*multiple-images*', which are dependent on the position along the waveguide section. This reflects the basic principle of MMI operation. Ulrich and Ankle [3] have showed the use of a ray optics technique to describe the self-imaging phenomenon, followed by the work of Chang and Kuester [4] who used a decomposition employing a Green's function technique. However, recently, Weinert *et al.*[5] used the finite difference-based beam propagation method (BPM) and a further analysis by Berry *et al.* [6] employed the semi-analytic Discrete Spectral Index (DSI) method to show the self-imaging nature of multimode interference based devices.

The intermodal coupling length, $L_{\pi n}$ between the first and the higher order modes of the MMI section can be calculated by using the relationship below :

$$L_{\pi n} = \frac{\pi}{\beta_0 - \beta_n} \quad (1)$$

where β_0 is the propagation constant of the first fundamental mode in the MMI section and β_n is the propagation constant of the n^{th} order mode in the same section. When the device length, L , is equal to $L_{\pi n}$, defined as one coupling length, self-imaging of the input field may be obtained. A careful consideration of the positioning of the input waveguides can lead to a wider MMI device, resulting in a reduction of its potential length.

However, in order to analyze these MMI-based devices, an accurate calculation of the modal solutions of the access waveguides and the multimode waveguide section is necessary. Although the effective index (EI) method is a simple and useful technique which may be used to calculate the propagation constants for simple structures, however, for the accurate characterization of complex MMI-based devices, the authors believe the

numerically versatile finite element method [7] is an ideal tool to calculate the modal field profiles, $\mathbf{H}(x,y)$, and their propagation constants, β .

In using the numerical approach presented here, an arbitrary incident field is decomposed into the guided modes of the MMI section and propagated along the length of the MMI. To determine the power carried by these modes, it is vital to be able to calculate the excited coefficients of the modes in the MMI section due to the incident mode via the input access waveguide. Most commonly, the simple overlap integral method [8] has been used to calculate the excited modal coefficients. By contrast, in the present work, it has been shown that the LSBR method is more accurate, as it satisfies the boundary conditions in the usual least squares sense over the interface. The LSBR method looks for a stationary solution by minimizing the error energy functional, J , given by [9]:

$$J = \int_{\Omega} |E_t^I - E_t^{II}|^2 + \alpha \cdot Z_0^2 |H_t^I - H_t^{II}|^2 d\Omega \quad (2)$$

to satisfy the necessary field continuity conditions. In this equation α is a dimensionless weighting factor to balance the electric and magnetic components of the error functional, J , Z_0 is the free-space impedance, and Ω is the interface across the junction.

In order to calculate the power output of the MMI device, the evolution of the field along the MMI can be calculated as a superposition of all the guided mode field distributions. By taking the phase of the fundamental mode (β_0) as a common factor out of the sum and assuming a time dependence, given by $\exp(j\omega t)$ and implicit hereafter, the field profile $\mathbf{H}(x,y,z)$ can be written as

$$\mathbf{H}(x, y, z) = \sum_{i=0}^{M-1} b_i \cdot \mathbf{H}(x, y) e^{-j(\beta_0 - \beta_i)z} \quad (3)$$

and similarly for the $\mathbf{E}(x,y,z)$ field. Here M is the total number of modes considered in the MMI section and b_i are the coefficients of the excited guided modes inside the MMI section.

3 The structure simulated

Figure 1 shows the layout of the structure simulated in this work. The MMI-based 3 dB coupler essentially simply consists of three major sections, which are classified as the input, MMI and the output sections, in which a single waveguide of $1.1\mu\text{m}$ width and $0.9\mu\text{m}$ height is used as the input access guide with a $0.3\mu\text{m}$ InP layer on top of the quaternary material, followed by MMI section of $9\mu\text{m}$ width, with all these guides being $0.9\mu\text{m}$ high. The output coupler configuration follows the same dimensions as the input with a separation of $1.9\mu\text{m}$ between the guides. A quaternary InGaAsP material of

bandgap $1.3\mu\text{m}$ was considered with an operating wavelength of $1.507\mu\text{m}$. In this simulation 12800

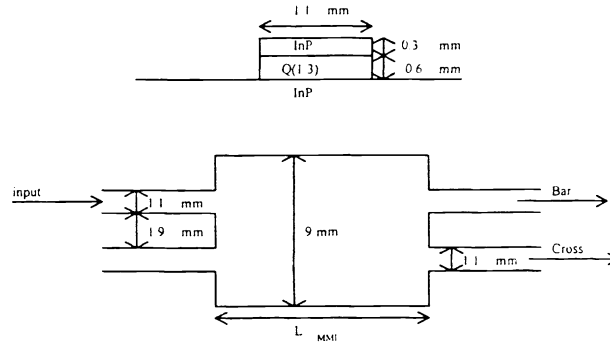


Fig.1 Schematic of the MMI simulated

first order elements were used. Table 1 shows the propagation constants and modal coefficients for the two-dimensional simulation obtained by using the vector finite element and the LSBR methods.

Modes	β	L_{cn}	τ (LSBR)	τ (OI)	ρ (LSBR)
$H_{y_{11}}$	13.81432	-----	0.40439	0.39439	0.80346E-2
$H_{y_{21}}$	13.80096	235.15	0.39406	0.38462	-----
$H_{y_{41}}$	13.71718	32.34	0.37660	0.36875	-----
$H_{y_{51}}$	13.70667	29.18	0.36347	0.35685	-----
$H_{y_{71}}$	13.59809	14.53	0.32199	0.31800	-----
$H_{y_{81}}$	13.52943	11.03	0.30831	0.30567	-----
$H_{y_{10,1}}$	13.36345	6.97	0.24913	0.24922	-----
$H_{y_{11,1}}$	13.26539	5.72	0.21894	0.22280	-----

Table 1 Propagation constants (β_n), Coupling lengths (L_{cn}) and Transmission coefficients (τ) for the planar MMI structure for a series of TE modes.

In this work the TE polarized wave has been considered unless mentioned otherwise. The modal coefficients obtained by the use of the simple overlap integral (OI) method are also included for comparison. It can be seen that the transmission coefficients (τ) values obtained by the LSBR method are always slightly higher than those using the OI method. The LSBR method, which satisfies the continuity condition by minimizing the error functional, J , and using the optimum weighting factor, α , is mathematically accurate, rigorously convergent and a powerful and versatile approach. The reflection coefficients, ρ , for the fundamental incident mode have been included as their estimation could be important for the characterization of many photonic devices, however this is difficult inaccurate or impossible using other simple methods. The CPU time for each modal solution is around 14 minutes using a Sun Classic Workstation. From the modal

parameters given in Table 1, the evolution of the field $\mathbf{H}(x,y,z)$ along the axial direction can be calculated. Figure 2 shows the field at the junction $Z=0_+$. This plot indicates clearly that at this position most of the power couples to the bar state, such as to match the incident field. The small ripples beyond the input guide are caused by incomplete cancellation from the superposition of the many modal fields excited in the MMI section, beyond the input guide width.

As the field propagates in the longitudinal z direction, it divides into two equal peaks at $z=115\mu\text{m}$, as shown in Figure 3. The two peaks reveal that the total power incident via the access waveguide is divided into equal portions at half the beat length, thus indicating the possibility of an MMI based 3 dB coupler, and Figure 4 reveals the power emerging from the output cross state at one coupling length, $L_C=230\mu\text{m}$, due to a 2π phase shift, compared to the field at the input, $z=0_+$.

Finally the power transfers to the bar and cross states are calculated by using the composite field at each axial location (z) and this is shown in Figure 5 for the 3 dB coupler as a function of the device length. From Figure 5 it can be observed that the bar and the cross states have 50% of the power that has been input to the MMI section, at around a length of $115\mu\text{m}$.

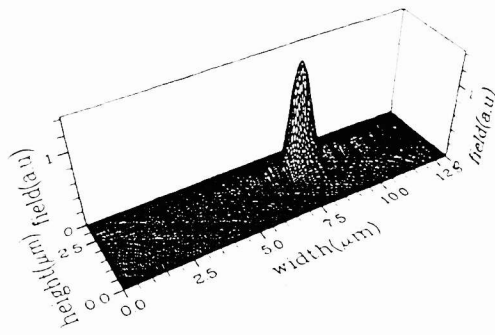


Fig. 2 Field at $z=0_+\mu\text{m}$

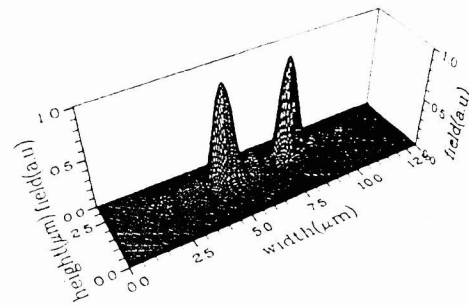


Fig.3 Field at half the L_C , $z=115\mu\text{m}$

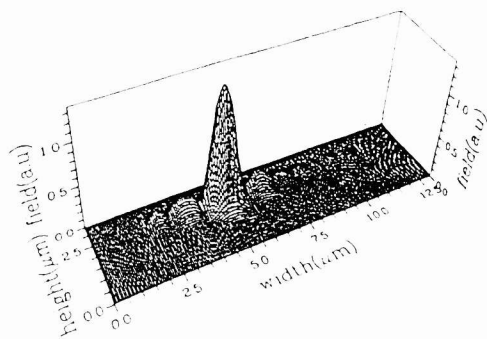


Fig. 4 Field at $L_C=230\mu\text{m}$

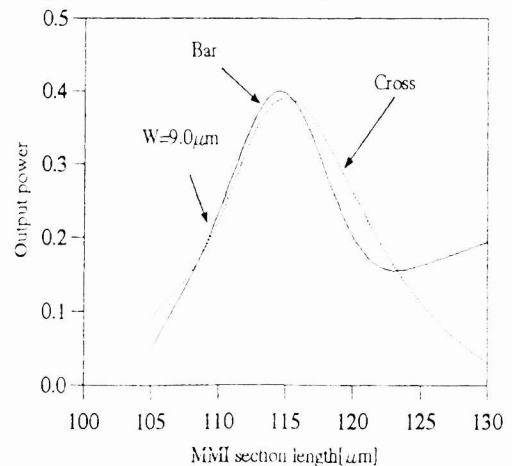


Fig. 5 Power coupling against the MMI length

This compares favourably with the experimental results obtained by Spikeman *et al.* [9] and confirms the reliability of the results of the numerical schemes presented here. However, a slight difference between the experimental results and the results of the simulation may also be attributed to the inaccuracy in the actual structural parameters including the refractive index values used. The authors considered that the modal propagation constants calculated by exploiting the symmetry and by using 12800 elements for half of the MMI waveguide section should be reasonably accurate for the subsequent calculation of the coupling lengths, and a much finer mesh, at an increased computational cost, could change the coupling length only slightly. This suggests that the numerical results presented here are highly accurate, given the structural data used in the simulation.

4 Fabrication tolerances

The effect of the fabrication tolerance for the MMI width is an important issue. For this study the width of the multimode section was increased by $0.5\mu\text{m}$ to $9.5\mu\text{m}$ from that used in the earlier section. The modal profiles for the MMI section were determined by using the FEM and the excited modal coefficients were calculated by using the LSBR. The composite field along the length of the multimode section was determined for the estimation of the power coupling to the two output waveguides. The power coupling efficiency of the new structure is shown in Fig.6, and it can be observed that the length required for the 3dB coupler has increased, since the intermodal coupling lengths were also increased.

Apart from that fact, it can be noticed that there is a higher imbalance between the bar and the cross states at the design length. This was due to the position of input and output waveguide sections as they were kept unchanged, as in the original design. Even though the possibility of having a tolerance of $0.5\mu\text{m}$ is unlikely in most of the fabrication processes, it has been chosen to indicate the importance of accurate design parameters to achieve better performance.

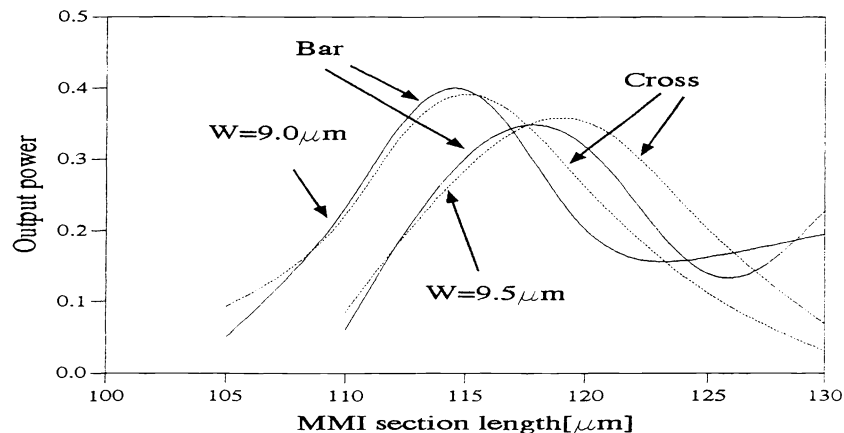


Fig. 6 Power transfer characteristics of the 3dB coupler for different MMI widths

4. Theory of the optical duplexer

Next, an optical duplexer using the *sol-gel* technique is characterized, such an optical duplexer can be designed by adjusting the device parameters and selecting the device length, L , where

$$L = mL_{\pi}(\lambda = 1.55\mu\text{m}) = nL_{\pi}(\lambda = 0.98\mu\text{m}) \quad (4)$$

The two wavelengths will emerge out of the bar and the cross states, respectively, when the device length is L , and m and n are odd or even integers.

5. Results for the duplexer

A schematic diagram of the two-dimensional MMI for the fully-integrated erbium-doped optical amplifier considered is shown in Figure 7.

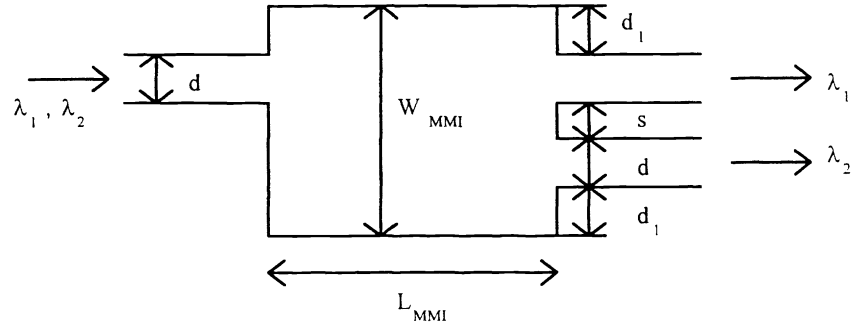


Fig. 7 Schematic of the MMI based duplexer

In this case the width of the single-mode input section was assumed to be $d=6\mu\text{m}$ and that of the MMI section was taken as $21\mu\text{m}$. The output guides were placed at $7\mu\text{m}$ and at $14\mu\text{m}$ for the case of '*restricted resonance*'. The output guide directly opposite the input is termed the '*bar state*' and the other output guide is termed the '*cross state*'. The refractive index of the guide was 1.502 and that of the substrate was 1.4507 at an operating wavelength of 980nm and at 1550nm the waveguide index was 1.4982 and that of the substrate was 1.444 [10]. This wavelength is very popular with the widespread use of the erbium-doped fiber amplifiers and it is used as the pump wavelength in erbium-doped integrated systems. Figure 8 shows the odd or even multiples of L_c versus the active layer thickness, plotted on a logarithmic scale.

From Fig.8 it can be seen that the two wavelengths intersect at an active layer thickness of $1.25\mu\text{m}$, and this value was taken for further simulations. The effect of material dispersion is also considered. Fig. 9 shows the power coupling efficiency on the output guide of the MMI for both the wavelengths considered.

It can be observed from Fig. 9 that around 88% of the power is in the bar state for $\lambda = 1550\text{nm}$. The little less efficiency of the 1550nm wavelength is due to the poor imaging of the input field which is caused due to the deviation from the quadrature relationship. However, from the power transfer curve it can be observed that even with losses of about 1dB , around 70% of power transfer is possible. It can also be observed that this design is less sensitive to the length as can be seen that for an axial variation of around $200\mu\text{m}$ both the wavelengths seems to transmit about 70% of the power. Fig. 10 shows the composite field profile at $z=5.2\text{mm}$ for the 1550nm wavelength.

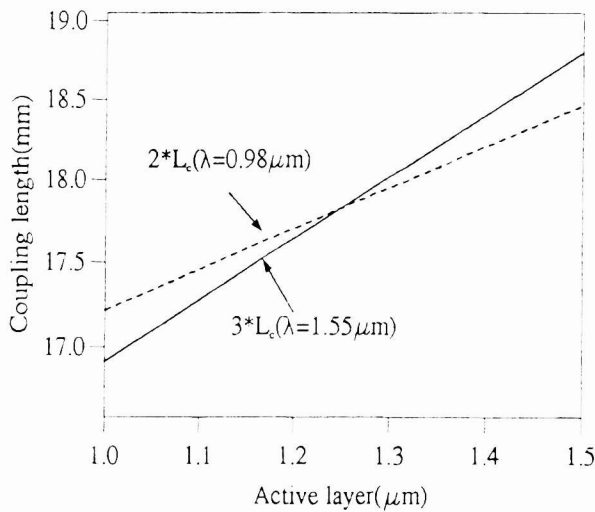


Fig. 8 Odd or even multiple of L_c versus active layer thickness

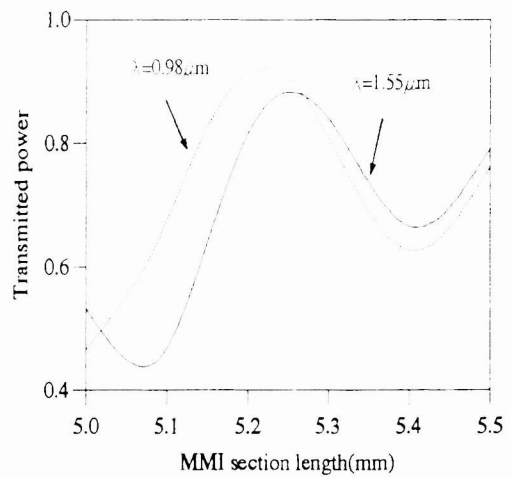


Fig. 9 Power coupling efficiency versus MMI length

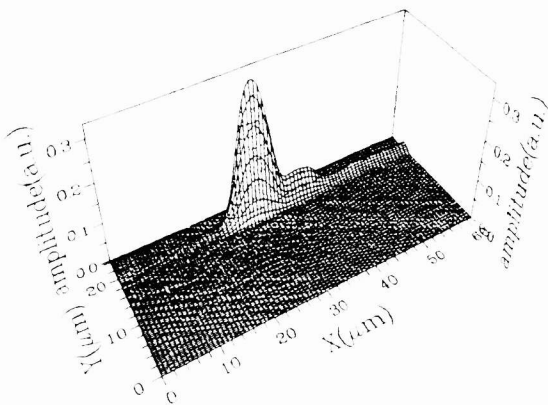


Fig.10 Composite field profile at $z=5.2\text{mm}$ for $\lambda=1550\text{nm}$

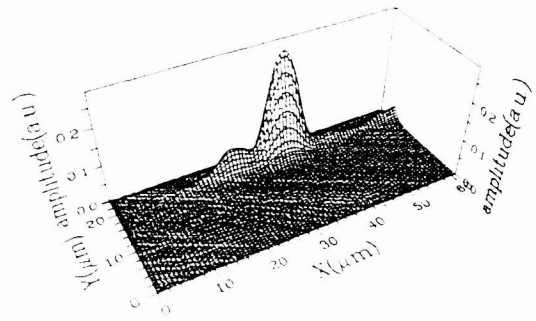


Fig. 11 Composite field profile at $z=5.2\text{mm}$ for $\lambda=980\text{nm}$

As can be seen from this figure most of the power is confined in the cross state. However, there is still some power left in the bar state, due to the incomplete cancellation of the input field. The higher deviation from the quadrature relationship can be improved by making the rib section slightly curved. This could improve the imaging slightly and hence a better coupling can be achieved.

Fig.11 shows the field in the bar state for the 980nm wavelength at $z=5.2\text{mm}$. It can be noticed from Fig. 11 that most of the power is in the bar state under these circumstances. It can also be noticed that the quality of the image is better here when compared to that of Figure 10, which shows that the quadrature relationship agrees better. This is due to the number of guided modes being higher at this wavelength and hence the device performance is better. Figure 12 shows the polarization property of the MMI for the 980nm wavelength. It can be noticed that the power coupling efficiency for the TM case is slightly better than the TE case.

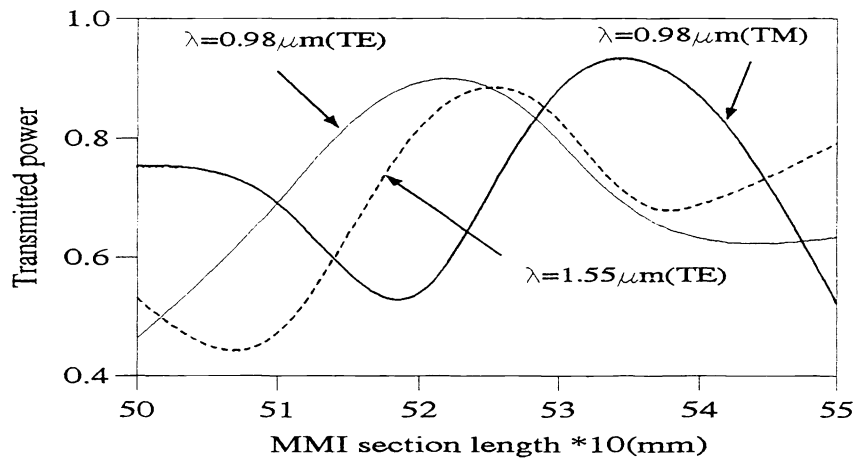


Fig. 12 Power coupling efficiency of the TE and the TM modes

Since there was around $17\mu\text{m}$ difference between the TE and the TM wave beat lengths, it can be noticed that there is an axial variation of $100\mu\text{m}$ between both the polarizations at the design length where the maximum power transfer occurs. From this simulation the length of the device is around 5.3mm whereas the same *sol-gel* technique employing the same dimensions as the MMI but employing the directional coupler technique resulted in a device length of 10.1mm [10].

6. Comparison of the performance of the MMI with directional coupler

In this section a rigorous comparison of the performance of a directional coupler with that of a MMI-based device is developed. To our knowledge, for the first time, the important properties such as cross-talk and polarization sensitivity are directly compared for both types of devices and their performance characteristics, developed in this simulation, are discussed.

A schematic of the structure simulated in this work, which can be fabricated using the *sol-gel* technique is shown in Fig. 13. P_b is the bar and P_c is the cross state of the directional coupler. The widths of the two identical coupled guides are $3\mu\text{m}$ and the

separation, S , between them may be varied. The MMI structure simulated in this study (not shown here), consists of a large multimode section of width W , and the input and output access waveguides which are of the same dimensions as the isolated waveguides of the directional couplers. The refractive index for the guide and substrate were taken as 1.4982 and 1.4440 respectively, at an operating wavelength of $1.55\mu\text{m}$.

Figure 14 shows the variation of the cross-talk with the device length (L) for the MMI and the directional couplers.

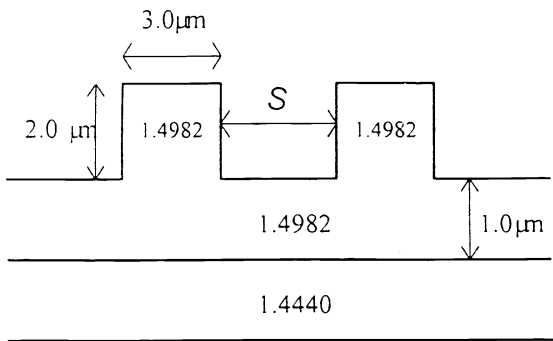


Fig. 13 Schematic of the directional coupler

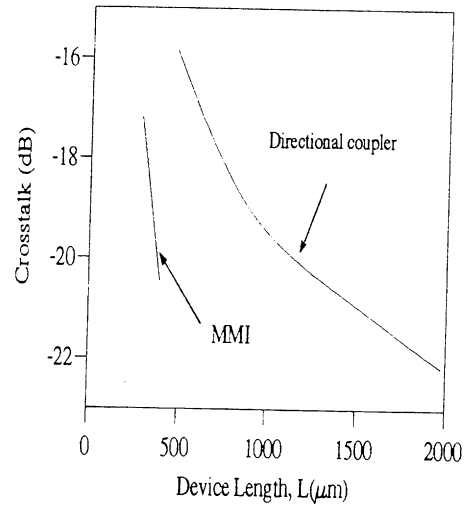


Fig. 14 The variation of the cross-talk against the device length for the MMI and the directional coupler

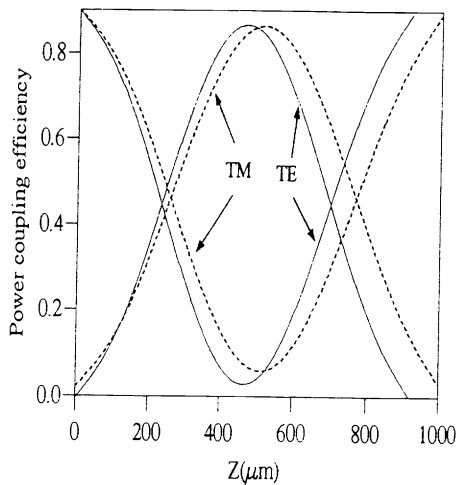


Fig. 15 Graph showing the polarization dependence of the directional coupler

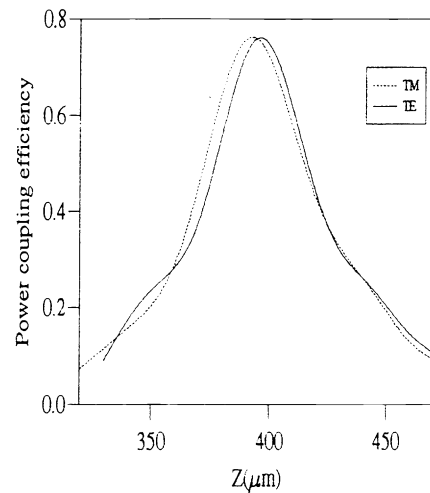


Fig. 16 Graph showing the power transfer efficiency for both the TE and the TM polarizations for the MMI

It can be observed that for both approaches, the cross-talk can be reduced by considering a longer device length. However, for a specific cross-talk requirement, the device length will be shorter if the MMI approach is used, as compared to the use of directional coupler-based devices. It can be also noticed from this figure that using the MMI approach, at half the device length as that of the directional coupler, the same cross-talk performance can be achieved. This is a crucial factor, since it not only proves the value of the shorter device length but also it shows that the same cross-talk can be achieved at a much shorter device length, by using the MMI-based approach. This suggests that the MMI-based devices have a better cross-talk performance when compared to directional coupler-based devices.

Next, the polarization sensitivity in the power transfer along the axial direction is studied. The polarization performance of these devices is important as most of the optical systems considered do not recognize the polarization state of the incoming signal. The variation of the power transfer efficiency along the axial direction for the directional coupler, with a separation of $1.0\mu\text{m}$, is shown in Figure 15. Results are shown for both the polarizations, where the solid and dashed lines indicate the TE and the TM polarizations respectively, whose coupling lengths were $467\mu\text{m}$ and $514\mu\text{m}$ respectively. At low separations between the guides, the excited coefficients of the two supermodes were slightly unbalanced and hence at the coupling length, a maximum of 86% of the input power transfer was coupled to cross-state for the TE polarization. However, at larger separations, the values of the excited coefficients become nearly equal and hence the maximum power transfer efficiency also increases, but however, the coupling lengths also increase. Even though the maximum power transfer is almost identical for both the polarizations, there is a difference of around $47\mu\text{m}$ in their coupling lengths. The power transfer efficiency is not very sensitive to the axial displacement, as it has been estimated that at an axial variation of $\pm 140\mu\text{m}$, the additional loss is only about 1dB less than its maximum value. At the TE coupling length, the TM power transfer is only 82% of the maximum for the TM polarization. When the device length equals the coupling length for the TE polarization, the cross-talk for TE and TM polarizations are -16dB and -12dB respectively.

Similarly, the polarization dependence of MMI-based devices is also studied. Figure 16 shows the TE and TM power transfer curves for the MMI structure considered here.

In this case there is only about $1\mu\text{m}$ difference between the beat lengths for these two polarizations, which represents only a 0.25% difference, whereas for a directional coupler, around 11% difference was observed. In the case of the MMI device, again, at maximum, around 77% of the input power transfer is possible. Here the lower power transfer is due to a strong discontinuity at the beginning of the MMI section. It can be seen that the axial distance tolerance is about $\pm 15\mu\text{m}$ for the power transfer to be within 1dB of the maximum. Although the power transfer efficiency of an MMI-based design is more sensitive along the axial direction, when compared to the directional coupler-based design, however it is clearly shown for both the cases that tolerance to the device length is not an important issue. This study shows that the MMI approach is almost polarization-insensitive whereas, by contrast, the directional coupler is highly polarization sensitive.

Conclusion

In this paper the authors have characterized several MMI based devices and studied their performance characteristics such as power coupling efficiency, polarization and fabrication tolerance. It is also shown that the MMI-based devices have a better cross-talk and polarization characteristics than the directional coupler based devices. The rigorous FEM and the LSBR methods have been shown as the most appropriate design tools for the characterization of such practical optoelectronic devices.

References

- [1] A. Chipouras, S. Markatos, T. Sphicopoulos, C. Caroubalos, Hans F. Mahlein, and R. Matz, " Performance Estimation and Yield Analysis of an OEIC Passive Duplexer," *J. Lightwave Technol.* **LT-14**, pp. 164-168, 1996.
- [2] L.B. Soldano and E.C.M. Pennings, " Optical Multi-mode Interference devices based on self-imaging : Principles and Applications," *J. Lightwave Technol.* **LT-13**, pp. 615-627, 1995.
- [3] R. Ulrich and G. Ankele, " Self-Imaging in homogeneous planar optical waveguides," *Appl. Phys. Lett.*, **Vol. 27**, pp.337-339, 1975.
- [4] D.C. Chang and E.F. Kuester, " A hybrid method for paraxial beam propagation in multimode optical waveguides, *IEEE Microwave Theory and Tech.*, **MTT-29**, pp. 923-933, 1981.
- [5] C.M. Weinert and N. Agrawal, " Three-dimensional finite difference simulation of coupling behaviour and loss in multimode interference devices," *IEEE Photonic Technol. Lett.*, **7**, pp.529-531, 1995.
- [6] G.M. Berry and S.V. Burke, " Analysis of optical rib self-imaging multimode interference (MMI) waveguide devices using the discrete spectral index method," *Opt. Quantum Electron.* **27**, pp. 529-531, 1995.
- [7] B.M.A. Rahman and J.B. Davies, " Finite element solution of integrated optical waveguides, " *J. Lightwave Technol.*, **LT-6**, pp.682-688, 1984.
- [8] B.M.A. Rahman and J.B. Davies, " Analysis of optical waveguide discontinuities," *J. Lightwave Technol.*, **LT-6**, pp.52-57, 1988.
- [9] L. H. Spikeman, Y.S. Oei, E.G. Metaal, F.H. Groen, I. Moerman and M.K. Smit, " Extremely Small Multimode Interference Couplers and Ultrashort Bends on InP by Deep Etching, " *IEEE Photonic Technol. Lett.*, **Vol.6**, No.4, pp. 1008-1010.
- [10] M.A. Forastiere, G.C Righini, and A. Verciani, " Design and numerical analysis of a "silica-on-silicon" integrated optical duplexer," *SPIE*, **Vol.2954**, pp.88-98, 1996